Amino Acids (2012) 43:219–232
DOI 10.1007/s00726-011-1066-0

ORIGINAL ARTICLE

Cyclic RGD peptides interfere with binding of the *Helicobacter pylori* protein CagL to integrins $\alpha_V\beta_3$ and $\alpha_5\beta_1$

Jens Conradi · Sylwia Huber · Katharina Gaus · Felix Mertink · Soledad Royo Gracia · Ulf Strijowski · Steffen Backert · Norbert Sewald

Received: 2 June 2011 / Accepted: 25 August 2011 / Published online: 14 September 2011

Abstract The human pathogen *Helicobacter pylori* that may cause different gastric diseases exploits integrins for infection of gastric cells. The *H. pylori* protein CagL present on the outer region of the type IV secretion pilus contains an RGD sequence (-Arg-Gly-Asp-) that enables binding to cells presenting integrins $\alpha_5\beta_1$ and $\alpha_V\beta_3$. This interaction can be inhibited with conformationally designed cyclic RGD peptides derived from the CagL epitope -Ala-Leu-Arg-Gly-Asp-Leu-Ala-. The inhibition of the CagL–$\alpha_V\beta_3$ interaction by different RGD peptides strongly suggests the importance of the RGD motif for CagL binding. CagL point mutants (RAD, RGA) show decreased affinity to integrin $\alpha_V\beta_3$. Furthermore, structure–activity relationship studies with cyclic RGD peptides in a spatial screening approach show the distinct influence of the three-dimensional arrangement of RGD motif on the ability to interfere with this interaction. Resulting from these studies, similar structural requirements for the CagL epitope as previously suggested for other ligands of integrin $\alpha_V\beta_3$ are proposed.

Keywords CagL · Integrins · $\alpha_V\beta_3$ · RGD peptides · SAR studies

Abbreviations

D-PBS	Dulbecco's phosphate buffered saline
DIPEA	Diisopropylethylamine
DMF	Dimethylformamide
EDTA	Ethylenediaminetetraacetic acid
HATU	1-[Bis-(dimethylamino)methyliumyl]-1H-1,2,3-triazolo[4,5-*b*]pyridine-3-oxide hexafluorophosphate
MEM	Minimum essential medium
MES	2-(*N*-Morpholino)ethanesulfonic acid
NMP	1-Methyl-2-pyrrolidone
Pbf	2,2,4,6,7-Pentamethyldihydrobenzofuran-5-ylsulfonyl

Electronic supplementary material The online version of this article (doi:10.1007/s00726-011-1066-0) contains supplementary material, which is available to authorized users.

J. Conradi · S. Huber · K. Gaus · F. Mertink · S. Royo Gracia · U. Strijowski · N. Sewald (✉)
Department of Chemistry, Bielefeld University, Universitätsstraße 25, PO Box 10 01 31, 33501 Bielefeld, Germany
e-mail: norbert.sewald@uni-bielefeld.de

Present Address:
S. Huber
F. Hoffmann-La Roche, Grenzacherstrasse 124, 4070 Basel, Switzerland

Present Address:
K. Gaus
Syngenta, Schaffhauserstrasse, 4332 Stein, Switzerland

Present Address:
S. Royo Gracia
Institute for Research in Biomedicine, Baldiri Reixac 10, 08028 Barcelona, Spain

Present Address:
U. Strijowski
German Institute of Food Technologies, Professor-von-Klitzing-Straße 7, 49610 Quakenbrück, Germany

S. Backert
School of Biomolecular and Biomedical Sciences, University College Dublin, Ardmore House, Belfield Campus, Dublin 4, Ireland

TBTU	3-[Bis(dimethylamino)methyliumyl]-3H-benzotriazol-1-oxide tetrafluoroborate
TFA	Trifluoroacetic acid
TIS	Triisopropylsilane

Introduction

Helicobacter pylori (*H. pylori*) is a micro-aerophilic human-specific Gram-negative bacterium that colonizes the stomach mucosa. *H. pylori* is able to persist in the stomach for many decades and even for a whole lifetime. More than half of the world's population is infected with this pathogen (Amieva and El-Omar 2008) that may cause gastric diseases such as chronic atrophic gastritis, peptic ulcers, mucosa-associated lymphoid tissue lymphoma, and noncardic gastric adenocarcinoma (Rieder et al. 2005).

Infection by *H. pylori* is correlated on the molecular level with secretion of pro-inflammatory cytokines as, e.g. interleukin-8 (IL-8), cell proliferation, and apoptosis of epithelial cells (Kwok et al. 2002). Although many post-infectious cellular pathways in an infected host cell are known in detail, the molecular mechanism of infection itself remains poorly understood. Strains of *H. pylori* may be divided in two classes, type I and II, and a classification relies on the presence or the absence of the *cag* PAI (*cytotoxin associated gene pathogenicity island*) in the genome of the bacterium (Asahi et al. 2000). Proteins encoded by the *cag* PAI play a crucial role in the pathogenicity of *H. pylori* strains (Amieva and El-Omar 2008; Rieder et al. 2005; Bourzac and Guillemin 2005; Backert and Meyer 2006). However, many of the virulence factors were found in both types of *H. pylori*. Virulent *H. pylori* possess a transport apparatus known as type IV secretion system consisting of a transmembrane secretion channel and an extracellular pilus (Rieder et al. 2005; Bourzac and Guillemin 2005; Backert and Meyer 2006; Cascales and Christie 2003; Backert et al. 2008). The type IV secretion system is responsible for injection of the oncoprotein CagA into host cells that causes changes in the signal transduction pathways and leads indirectly to a diversity of subsequent disease developments (Backert and Meyer 2006; Cascales and Christie 2003; Backert et al. 2000, 2008; Asahi et al. 2000).

Pathogenic viruses and microorganisms are known to exploit integrins ($\alpha_V\beta_1$, $\alpha_V\beta_3$, $\alpha_V\beta_5$, $\alpha_V\beta_6$, $\alpha_3\beta_1$, $\alpha_4\beta_1$, $\alpha_5\beta_1$, $\alpha_6\beta_1$) for attachment to the target cell (Backert et al. 2008; Sheppard 2003; Isberg and Barnes 2001; Stewart and Nemerow 2007). For example, integrin $\alpha_V\beta_5$ is one of several *Adenovirus* receptors that mediate productive infection in cultured cells promoting virus internalization and endosome release (Wickham et al. 1994; Sheppard 2003). The three integrins $\alpha_V\beta_1$ (Jackson et al. 2002), $\alpha_V\beta_3$, and $\alpha_V\beta_6$ (Jackson et al. 2000) are involved in infection of cloven-hoofed animals by *foot and mouth disease virus* (FMDV). The pathogen *Yersinia pseudotuberculosis* exploits gastric M cells in interacting with its bacterial protein invasin as ligand for $\alpha_3\beta_1$, $\alpha_4\beta_1$, $\alpha_5\beta_1$, and $\alpha_6\beta_1$ integrins (Isberg and Leong 1990). Such a direct interaction of bacterial proteins with integrins constitutes one pathway for infection, while other microorganisms indirectly address integrins with bacterial fibronectin-binding proteins (Hoffmann et al. 2011).

Integrins, heterodimeric cell surface receptors, consist of an α and a β subunit. Molecular recognition between these surface receptors and their natural ligands contribute to many physiological phenomena mediating, e.g. cell adhesion, migration, and survival (Meyer et al. 2006; Kwok et al. 2007). Pathological processes mediated by integrins comprise tumor-induced angiogenesis (Serini et al. 2006), chronic inflammation, heart failures, and cancer metastasis (Sheppard 2003; Ruoslahti 1996; Isberg and Tran Van Nhieu 1994).

Integrin–ligand interaction in many cases is mediated by a short amino acid sequence, often a tripeptide, which is localized on the surface of the ligand. The RGD (-Arg-Gly-Asp-) tripeptide epitope is the most important recognition motif of integrins (Eble and 1997) that is recognized by α_V integrins and also by $\alpha_5\beta_1$ (Meyer et al. 2006). The discovery of short recognition sequences of integrins has led to the development of ligands that may interfere in the interaction between integrins and their natural protein ligands and are applied as potential therapeutics in the therapy of integrin-mediated diseases (Pierschbacher et al. 1981; Ruoslahti and Pierschbacher 1987; Mas-Moruno et al. 2010).

CagL of *H. pylori* is a 27-kDa protein predicted to adopt mainly α-helical structure (Backert and Selbach 2008) that contains the epitope ALRGDLA in a flexible loop (Fig. 1) where the RGD sequence was hypothesized to act as a recognition motif for host cell integrins (Kwok et al. 2007).

We have recently demonstrated in surface plasmon resonance studies and functional investigations that *H. pylori* CagL interacts with integrin $\alpha_5\beta_1$ and that the infection of gastric epithelial cells by *H. pylori* is mediated by the interaction of CagL on the pilus surface with integrin $\alpha_5\beta_1$ localized on the surface of gastric epithelial cells (Kwok et al. 2007). Besides $\alpha_5\beta_1$, other RGD recognizing integrins such as $\alpha_V\beta_3$ and $\alpha_V\beta_5$ are likely target structures of CagL. However, a recent publication questions RGD-dependent binding of CagL to β_1 integrins (Jiménez-Soto et al. 2009). Instead, data on RGD-independent binding of CagA (that lacks an RGD sequence) to $\alpha_5\beta_1$ have been presented.

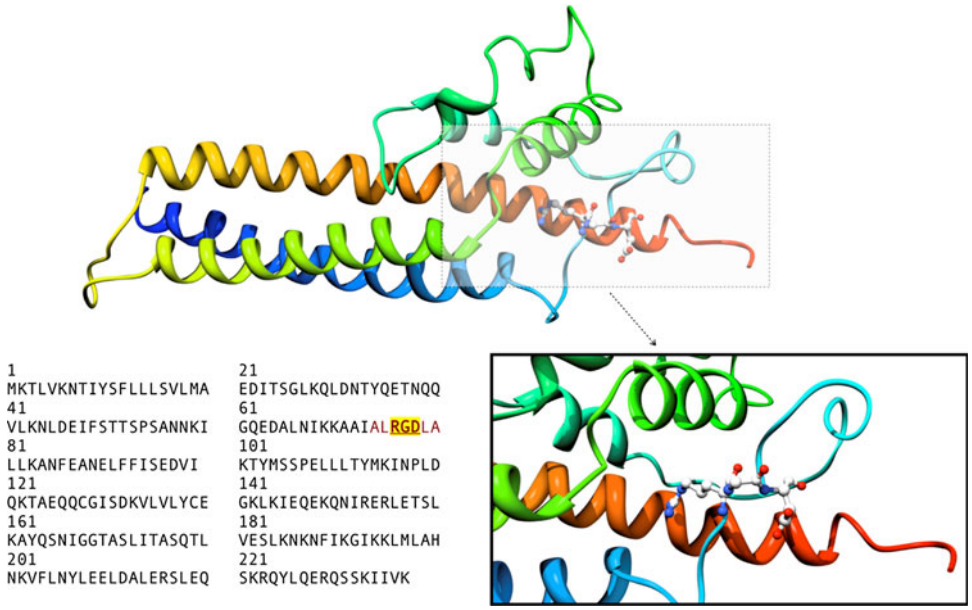

Fig. 1 Comparative protein structure model of CagL (Backert and Selbach 2008) showing the Arg-Gly-Asp motif exposed in a very flexible loop. The proposed structure of CagL is mainly α-helical

We examined the interaction of recombinant *H. pylori* CagL in cell adhesion assays with the cell line WM-115, which is considered a model cell line expressing integrins $\alpha_V\beta_3$, $\alpha_V\beta_5$, and $\alpha_5\beta_1$. Besides screening the inhibitory capacity of different antibodies, we synthesized a series of cyclic penta- and hexapeptides mimicking the CagL-binding epitope -Ala-Leu-Arg-Gly-Asp-Leu-Ala- to investigate the structural requirements of cyclic RGD peptides for inhibition of binding of CagL to integrins $\alpha_V\beta_3$, $\alpha_V\beta_5$, and $\alpha_5\beta_1$. The sequence-specific incorporation of D-amino acids into the peptides induced predictable solution structure. The peptide conformations were determined using NMR and MD calculations. The inhibitory capacity of the peptides on the CagL-integrin interaction was determined in cell adhesion assays.

Materials and methods

Peptide synthesis

Fmoc-α-amino acids were purchased from IRIS Biotech (Marktredwitz, Germany) and Advanced ChemTech (Louisville, USA). A dual-channel syringe pump (KD Scientific Inc., Holliston, USA) was used for slow reagent addition. MALDI-ToF MS analyses were performed on a Voyager-DE (Perseptive Biosystems, Foster City, USA) using 2,5-dihydrobenzoic acid as the matrix. Preparative RP-HPLC was performed on a Thermo Separation Products apparatus equipped with a Jupiter C18 (350 Å, 10 µm, 250 × 21.2 mm) efficiency column (Phenomenex, Torrance, USA) with water/acetonitrile gradients as the eluent and UV detection at 220 nm. Analytical RP-HPLC was performed on a Thermo Separation Products apparatus equipped with a Hypersil Gold (3 µm, 150 × 2.1 mm) column (Thermo Fisher Scientific, Walthan, USA) with water/acetonitrile gradients as the eluent and UV detection at 220 nm. Eluent A: 95% water, 5% acetonitrile, 0.1% TFA; Eluent B: 95%, acetonitrile 5% water, 0.1% TFA; 0.7 ml min^{-1}, 0–5 min 100% A → 100% B; 5–6 min 100% B → 100% A; 6–6.5 min 100% A.

Linear peptides were synthesized by solid-phase peptide synthesis on a Liberty 12-channel microwave-assisted automated peptide synthesizer (CEM, Matthews, USA) according to a Fmoc-protocol with 2-chlorotrityl resin (IRIS Biotech, Marktredwitz, Germany) as solid support. The C-terminal, resin-bound amino acids were Gly for cyclopeptides **1–6** and D-Leu for cyclopeptide **7,** respectively (loading 0.8 mmol/g). In a typical experiment, each peptide coupling was done with 3 equiv. Fmoc-amino acid (0.5 M in DMF), 3 eq. TBTU (0.5 M in DMF), and 6 eq. DIPEA (2 M in NMP). After washing with DMF the Fmoc group was cleaved with a solution of 20% piperidine in DMF. After complete assembly of the linear peptide it was cleaved from the resin using a solution of 1% (TFA) in dichloromethane. The resin was treated with this solution 10 times for 5 min each. After cleavage from the resin, the peptides were cyclized under pseudo-high dilution conditions (Malešević et al. 2004). 200 µmol of linear precursor was dissolved in 20 mL DMF and transferred into a syringe. 600 µmol HATU was dissolved in the same volume of DMF and transferred into a second syringe. These two solutions were added to a stirred solution of 1200 µmol DIPEA and 20 µmol HATU in 10 mL DMF at a rate of 1.00 mL h^{-1}(Malešević et al. 2004). Once the addition was complete, the mixture was stirred for further 15 min. The

solvent was evaporated under reduced pressure at a temperature lower than 30°C and the peptide was purified using preparative RP-HPLC. A cleavage cocktail consisting of TFA (95%), TIS (2.5%), and water (2.5%) was added to the cyclic protected peptide. The solution was shaken at room temperature for 8 h, the solvent was evaporated, and cold diethyl ether (30 mL) was added to the residue. Diethyl ether was decanted, centrifuged for 1 h at 0°C with 4,000×*g*, and again decanted. The residue was dissolved in water, lyophilized, and purified by preparative RP-HPLC.

Cell culture

The epithelial melanoma cell line WM-115 (ATCC, Wesel, Germany; CRL-1675™) was cultivated in MEM medium (PAA, Pasching, Austria) supplemented with 10% fetal bovine serum and 50 μg mL^{-1} gentamycin (PAA, Pasching, Austria). Cells were cultivated at 37°C and 5.3% (v/v) CO_2 and subcultivated in a ratio of 1:3 to 1:5 every 2–3 days.

Cell adhesion assays

Competition assays were performed with WM-115 human epithelial cancer cells. Therefore, WM-115 cells were cultivated to a confluence of 70%, detached with Trypsin-EDTA (0.05%/0.02% in D-PBS) (PAA, Pasching, Austria), washed with MEM medium, resuspended in MEM medium with 1 mg mL^{-1} fluorescein diacetate (Sigma-Aldrich, St. Louis, USA) to a cell density of 1×10^5 cells mL^{-1}, and incubated at 37°C under steady shaking for 30 min. Subsequently, cells were washed two times with MEM medium, resuspended with MEM medium containing divalent cations Ca^{2+} and Mg^{2+} (2 mM) to obtain a cell density of 1×10^5 cells mL^{-1} and incubated in the dark on ice for 30 min.

For the cell adhesion assay $CagL^{WT}$ was immobilized on a Nunc Maxisorp™ surface and WM-115 cells pre-incubated with varying concentrations of fibronectin were dispensed to the immobilized $CagL^{WT}$. Likewise, WM-115 cells were pre-incubated with different $CagL^{WT}$ concentrations before adding to immobilized fibronectin.

The cell suspension was added to the peptide solutions to give concentrations ranging from milimolar to nanomolar and incubated 30 min at 37°C. It was then dispensed on the coated microtiter plate ($5 \cdot 10^4$ cells $well^{-1}$) and incubated for 1 h at 37°C. Unbound cells were aspirated and bound cells were washed twice with MEM medium. Fluorescence was measured (λ_{ex} 485 nm; λ_{em} 514 nm) in an Infinite™ 200 Microplate Reader (Tecan, Männedorf, Switzerland). IC_{50} values (50% cell binding inhibition) of the tested peptides were evaluated with the GraphPad Prism 4.03 software (GraphPad, San Diego, USA).

In cell adhesion assays the murine monoclonal antibodies LM609 (EMD Millipore, Billerica, USA) against human integrin $\alpha_V\beta_3$, 3S3 (AbD Serotec, MorphoSys AG, Germany) against β_1 integrin, and P1F6 (EMD Millipore, Billerica, USA) against $\alpha_V\beta_5$ were used in final concentrations of 25 μg mL^{-1}. The assay was performed as described above. Instead of staining the cells with fluorescein diacetate, they were washed with Puck's salt solution (5.4 mM KCl, 0.4 mM KH_2PO_4, 5.6 mM D-glucose, 136 mM NaCl, 2 mM $MgCl_2$, 2 mM $MnCl_2$), fixed for 30 min at room temperature using 5% (w/v) glutaraldehyde, and stained with crystal violet 1% (w/v) in 100 mM MES (pH 6.0) over 60 min at room temperature. After a second washing step with Puck's salt solution, 100 mM citric acid in ethanol was added and the cells were incubated 30 min at room temperature for visualization. Absorption was measured using the Infinite™ 200 Microplate Reader at 560 nm.

NMR structure determination

NMR measurements were carried out at 300 K in DMSO-D_6 solutions containing 5–10 mM peptide using an Avance DRX-600 spectrometer (14.1 T) (Bruker, Karlsruhe, Germany), with a ^1H resonance frequency of 600.13 MHz and a ^{13}C resonance frequency of 150.90 MHz. Correlated spectra were recorded using inverse 5 mm probes, either TBI or TXI with z gradient. A TXO probe was used for ^{13}C measurements. Assignment of chemical shifts was based on phase-sensitive double-quantum-filtered correlation spectra (DQF-COSY, Rance et al. 1983), total correlation spectra (TOCSY) with a DIPSI pulse sequence for homonuclear Hartmann-Hahn transfer (Shaka et al. 1988; Bax and Davis 1985a), heteronuclear correlated inverse single-quantum correlation (HSQC, Kay et al. 1992), and heteronuclear multiple-bond correlation spectroscopy (HMBC, Bax and Summers 1986). Distance restraints were derived from NOESY spectra (Macura et al. 1981). In order to ensure linear NOE buildup rates, the intensities of selected peaks at different mixing times were determined. Phase-sensitive ROESY spectra were recorded to detect chemical exchange (Bax and Davis 1985b). Temperature gradients of the chemical shifts of the amide protons were measured by recording either ^1H NMR spectra or DQF-COSY spectra at different temperatures (295, 300, 305, 310, 315, and 325 K). The experiments carried out for the peptides and the acquisition and processing parameters are compiled in Table S1. Spectra were acquired and processed using Topspin software (Bruker, Karlsruhe, Germany). Assignment and integration of the NOE spectra was accomplished with the software Sparky (Goddard et al. "Sparky 3"). The chemical shifts assigned for the different peptides are listed in Tables 1, 2, 3, 4, 5, and 6.

Table 1 ^{1}H-NMR and ^{13}C-NMR chemical shifts of c-(-Arg-Gly-Asp-D-Leu-Ala-) **2** in DMSO-D_6

Residue	δ/ppm						
	H^N	H^α	H^β	H^γ	H^δ	H^ε	
Arg-1	7.85	4.18	1.56/1.76	1.41	3.10	7.57	
Gly-2	8.24	3.24/4.10					
Asp-3	7.96	4.58	2.44/2.63				
D-Leu-4	7.82	4.32	1.38/1.47	1.53	0.87		
Ala-5	8.30	4.13	1.26				
	C	C^α	C^β	C^γ	C^δ	C^ζ	N	N^ε
Arg-1	171.5	52.3	28.3	25.6	40.9	157.1	113.2	145.3
Gly-2	169.6	43.8					109.2	
Asp-3	170.8	49.4	36.2				120.0	
D-Leu-4	172.1	51.4	41.0	24.6	22.4/23.4		120.4	
Ala-5	173.2	50.8	18.3				122.5	

c-(-Arg-Gly-Asp-D-Leu-Ala-) **2** yield: 19%; purity: 98% analyt. RP-HPLC: $t_R = 2.4$ min. MALDI-ToF MS: 513.68 ($M + H^+$, calcd.: 513.28), 535.69 ($M + Na^+$, calcd.: 535.27), 551.65 ($M + K^+$, calcd.: 551.24)

Table 2 ^{1}H-NMR and ^{13}C-NMR chemical shifts of c-(-Arg-Gly-Asp-Leu-D-Ala-) **3** in DMSO-D_6

Residue	δ/ppm						
	H^N	H^α	H^β	H^γ	H^δ	H^ε	
Arg-1	8.04	4.26	1.48/1.72	1.48	3.10	7.55	
Gly-2	8.20	3.61/3.73					
Asp-3	8.60	4.29	2.56/2.62				
Leu-4	7.30	4.28	1.36/1.53	1.45	0.86		
D-Ala-5	8.60	4.29	1.15				
	C	C^α	C^β	C^γ	C^δ	N	N^ε
Arg-1	172.5	52.6	28.9	25.7	40.8	119.8	144.9
Gly-2	169.9	43.2				109.0	
Asp-3	171.2	52.5	36.2	171.9		123.3	
Leu-4	172.2	51.4	41.5	24.9	22.8/23.1	114.1	
D-Ala-5	172.6	48.7	15.7			128.0	

c-(-Arg-Gly-Asp-Leu-D-Ala-) **3** yield: 38%; purity: >99% analyt. RP-HPLC: $t_R = 2.4$ min. MALDI-ToF MS: 513.63 ($M + H^+$, calcd.: 513.28), 535.56 ($M + Na^+$, calcd.: 535.27), 551.40 ($M + K^+$, calcd.: 551.24)

Table 3 ^{1}H-NMR and ^{13}C-NMR chemical shifts of c-(-Arg-Gly-Asp-D-Leu-Ala-Leu-) **4** in DMSO-D_6

Residue	δ/ppm						
	H^N	H^α	H^β	H^γ	H^δ	H^ε	
Arg-1	8.42	3.79	1.57/1.64	1.39/1.49	3.10	7.53	
Gly-2	8.62	3.40/3.86					
Asp-3	7.99	4.54	β^2: 2.44 β^3: 2.53				
D-Leu-4	8.55	4.09	1.45	1.57	0.83/0.90		
Ala-5	8.61	4.04	1.24				
Leu-6	7.60	4.36	1.41/1.64	1.67	0.89		
	C	C^α	C^β	C^γ	C^δ	N	N^ε
Arg-1	172.6	55.2	27.1	25.8	40.8	119.4	144.9
Gly-2	169.6	43.3				109.7	
Asp-3	170.7	50.3	35.8	172.3		114.9	
D-Leu-4	171.6	53.4	39.4	24.7	22.9/23.4	125.9	
Ala-5	173.2	49.4	18.0			124.5	
Leu-6	173.9	50.2	41.1	24.8	23.4	113.5	

c-(-Arg-Gly-Asp-D-Leu-Ala-Leu) **4** yield: 15%; purity: 99% analyt. RP-HPLC: $t_R = 2.7$ min. MALDI-ToF MS: 626.99 ($M + H^+$, calcd.: 626.38), 648.97 ($M + Na^+$, calcd.: 648.37), 664.96 ($M + K^+$, calcd.: 664.34)

Table 4 ^{1}H-NMR and ^{13}C-NMR chemical shifts of c-(-Arg-Gly-Asp-Leu-D-Ala-Leu-) **5** in DMSO-D_6

Residue	δ/ppm							
	H^N	H^α	H^β		H^γ	H^δ		H^ε
Arg-1	7.44	4.30	1.57/1.69		1.39	3.09		7.57
Gly-2	8.55	3.42/3.82						
Asp-3	8.48	4.42	β^2: 2.61 β^3: 2.73					
Leu-4	7.43	4.34	1.53		1.52	0.84/0.88		
D-Ala-5	8.02	4.21	1.14					
Leu-6	8.38	4.07	1.47/1.57		1.61	0.81/0.88		
	C	C^α	C^β	C^γ	C^δ	C^ζ	N	N^ε
Arg-1	171.8	52.1	30.2	25.4	40.8	157.1	114.6	145.1
Gly-2	169.7	43.9					109.2	
Asp-3	170.6	50.8	36.3	172.3			118.6	
Leu-4	171.4	51.4	41.9	24.7	22.7		112.7	
D-Ala-5	172.8	49.1	17.4				122.8	
Leu-6	172.2	52.3	40.4	24.9	21.5/23.5		118.6	

c-(-Arg-Gly-Asp-Leu-D-Ala-Leu) **5** yield: 31%; purity: >99% analyt. RP-HPLC: t_R = 2.7 min. MALDI-ToF MS: 626.55 ($M + H^+$, calcd.: 626.38), 648.87 ($M + Na^+$, calcd.: 648.37), 664.93 ($M + K^+$, calcd.: 664.34)

Table 5 ^{1}H-NMR and ^{13}C-NMR chemical shifts of c-(-Arg-Gly-Asp-Leu-Ala-D-Leu-) **6** in DMSO-D_6

Residue	δ/ppm					
	H^N	H^α	H^β	H^γ	H^δ	H^ε
Arg-1	8.53	4.23	1.47/1.95	1.43/1.49	3.08	7.55
Gly-2	8.05	3.71/4.08				
Asp-3	8.18	4.19	2.53/2.59			
Leu-4	8.08	4.27	1.42/1.60	1.54	0.81/0.88	
Ala-5	7.36	4.27	1.18			
D-Leu-6	8.51	4.02	1.46/1.53	1.55	0.86/0.93	
	C	C^α	C^β	C^γ	C^δ	C^ζ
Arg-1	172.1	52.5	28.0	25.8	40.8	157.2
Gly-2	168.9	41.7				
Asp-3	171.5	52.2	36.2			
Leu-4	172.0	52.2	41.2	24.6	21.6/23.5	
Ala-5	173.2	48.5	19.9			
D-Leu-6	172.3	53.4	39.6	24.7	22.7	

c-(-Arg-Gly-Asp-Leu-Ala-D-Leu) **6** Yield: 24%; purity: >99% analyt. RP-HPLC: t_R = 2.8 min. MALDI-ToF MS: 626.84 ($M + H^+$, calcd.: 626.38), 648.85 ($M + Na^+$, calcd.: 648.37), 664.82 ($M + K^+$, calcd.: 664.34)

Table 6 ^{1}H-NMR and ^{13}C-NMR chemical shifts of c-(-Arg-Ala-Asp-D-Leu-Ala) **7** in DMSO-D_6

Residue	δ/ppm					
	H^N	H^α	H^β	H^γ	H^δ	H^ε
Arg-1	7.80	4.06	1.69	1.38/1.45	3.10	7.55
Ala-2	8.10	4.05	1.27			
Asp-3	8.05	4.39	2.45/2.77			
D-Leu-4	8.07	4.30	1.42	1.52	0.86	
Ala-5	8.17	4.06	1.25			
	C	C^α	C^β	C^γ	C^δ	C^ζ
Arg-1	171.0	54.4	28.7	25.8	40.8	157.1
Ala-2	172.4	51.0				
Asp-3	170.2	50.2	35.8	172.3		
D-Leu-4	171.8	51.6	40.8	24.7	22.7/23.6	
Ala-5	172.9	50.6	18.0			

c-(-Arg-Ala-Asp-D-Leu-Ala-) **7** yield: 12%; purity: >99% analyt. RP-HPLC: t_R = 2.4 min. MALDI-ToF MS: 527.70 ($M + H^+$, calcd.: 527.30), 549.86 ($M + Na^+$, calcd.: 549.29), 565.88 ($M + K^+$, calcd.: 565.36)

In the case of the pentapeptides c-(-Arg-Gly-Asp-D-Leu-Ala-) **2** and c-(-Arg-Gly-Asp-Leu-D-Ala-) **3**, NOESY spectra at 400 ms mixing time were integrated, in the case of hexapeptides c-(-Arg-Gly-Asp-D-Leu-Ala-Leu-) **4**, c-(-Arg-Gly-Asp-Leu-D-Ala-Leu-) **5** and c-(-Arg-Gly-Asp-Leu-Ala-D-Leu-) **6**, NOESY spectra at 350 ms mixing time were used to derive distance restraints. For control cyclopeptide c-(-Arg-Ala-Asp-D-Leu-Ala-) **7** sufficient distance restraints could not be obtained by NOESY; therefore, ROESY with offset correction was used. The restraints are listed in the Supplementary Material, Tables S2–S7. Pseudoatoms were used for non-assigned diastereotopic atoms and are listed according to IUPAC nomenclature (Markley et al. 1998). The observed distances were used as restraints in distance geometry (DG) calculations combined with a simulated annealing (SA) step (Xplor-NIH, Schwieters et al. 2003) to generate 1,000 structures, which were clustered according to their torsion angles (Guthöhrlein et al. 2007).

The central structures of the resulting clusters were used as starting structures in restrained molecular dynamics (MD) calculations (2.5 ns, GROMOS96/++, Schuler et al. 2001), GROMOS 45a3d force field, Geerke et al. 2004). The simulation was carried out in a truncated octahedral solvent box with explicit solvent molecules and a minimum distance between the solute atoms and the box border of 1.6 nm. Time-averaged distance restraints were applied. Temperature coupling of solvent and solute to an external bath of 300 K was weak with a relaxation time of 0.1 ps. A constant pressure of 1 atm with a relaxation time of 0.5 ps and an isothermal compressibility of 4.575×10^{-4} kJ mol^{-1} nm^{-3} was applied to the system. For the constriction of the bond length, a SHAKE algorithm with a geometric tolerance of 10^{-2} pm was applied. The equations of motion were integrated with the leapfrog algorithm and a time step of 2 fs. The resulting trajectories were clustered according to their torsion angles. In cases, where several restrained MD calculations were performed and similar clusters could be observed for the different trajectories, trajectories were combined and clustered together. The central structures were applied as starting structures in unrestrained MD calculations (10 ns, similar protocol as for restrained MD). A final torsion angle clustering step led to the structure proposals. An overview of the workflow for the structural determination that was established by Huber and Guthöhrlein is shown in Supplementary Material Figure S1.

Results

Although the relevance for the interaction between CagL and integrin $\alpha_5\beta_1$ has been clearly shown, the interaction of CagL with other integrins has not been addressed before. The aim of our study was to identify other integrins as putative interaction partners of CagL and to elucidate the binding epitope in order to improve the understanding of the interaction of the *H. pylori* protein CagL with integrins. We chose an approach combining techniques of Chemical Biology and Biochemistry for that purpose. Like integrin $\alpha_5\beta_1$, integrin $\alpha_V\beta_3$ recognizes the tripeptide epitope -Arg-Gly-Asp- in its ligands, among them the extracellular matrix proteins vitronectin and fibronectin (Charo et al. 1990).

The cell line WM-115 was chosen as $\alpha_V\beta_3$ expressing model for the cell adhesion assays. For this cell line integrin expression was investigated with reverse transcriptase PCR and protein immunoblotting. WM-115 is considered as a model cell line mainly expressing $\alpha_5\beta_1$, $\alpha_V\beta_3$, and $\alpha_V\beta_5$. In addition, the functionally blocking monoclonal antibody LM609 (EMD Millipore, Billerica, USA) against human integrin $\alpha_V\beta_3$ was incubated with WM-115 cells and the adhesion to immobilized $CagL^{WT}$ was tested, showing an inhibition by 50% (Fig. 2). We, therefore, conclude that CagL interacts not only with integrin $\alpha_5\beta_1$ (Kwok et al. 2007), but also with integrin $\alpha_V\beta_3$. The adhesion of WM-115 cells to $CagL^{WT}$ was reduced by 35% with the monoclonal antibody 3S3 (AbD Serotec, MorphoSys AG, Germany) against β_1 integrin, while the antibody P1F6 (EMD Millipore, Billerica, USA) against $\alpha_V\beta_5$ displayed only weak inhibition. These results indicate a complex interaction of $CagL^{WT}$ with the different integrin receptors of WM-115 cells. The effect of antibody LM609 emphasizes the importance of the $CagL^{WT}$ interaction with integrin $\alpha_V\beta_3$. The pre-incubation of WM-115 cells with

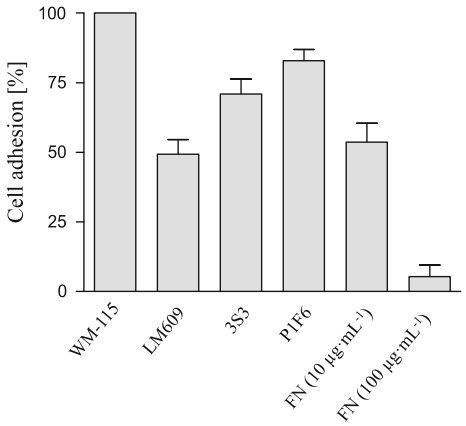

Fig. 2 Adhesion of WM-115 cells to immobilized $CagL^{WT}$ after pre-incubation of the cells with murine antibodies LM609, 3S3, and P1F6, specific against human integrins $\alpha_V\beta_3$, β_1, and $\alpha_V\beta_5$, respectively. The data indicate a complex interaction pattern of $CagL^{WT}$ with the different surface-exposed integrins of WM-115 cells. Pre-incubation of the cells with fibronectin shows a concentration dependent competition of the $CagL^{WT}$-integrin interaction

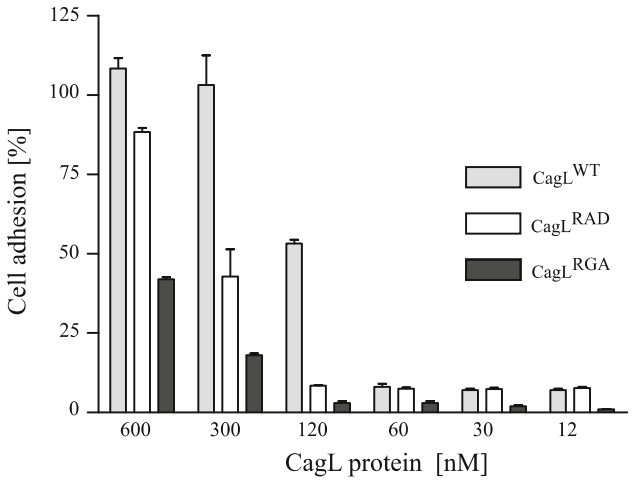

Fig. 3 WM-115 cells expressing integrin $\alpha_V\beta_3$ still adhere to the immobilized mutated proteins $CagL^{RAD}$ and $CagL^{RGA}$, albeit with reduced affinity compared with immobilized $CagL^{WT}$

10 μg mL^{-1} (0.04 μM) and 100 μg mL^{-1} (0.4 μM) fibronectin led to a significant concentration-dependent decrease of cell adhesion, which suggests competition of fibronectin with the $CagL^{WT}$ for integrin receptor binding sites.

We further investigated the relevance of the intact RGD tripeptide epitope of $CagL^{WT}$ for binding to WM-115 cells. Interestingly, the WM-115 cells still adhered to immobilized $CagL^{RAD}$ and $CagL^{RGA}$, where the RGD sequence was mutated to RAD and RGA, albeit with reduced affinity (Fig. 3). Cell adhesion to the mutant proteins $CagL^{RAD}$ and $CagL^{RGA}$ was distinctly different. The lower affinity to the $CagL^{RGA}$ mutant compared with $CagL^{RAD}$ highlights the importance of the aspartate residue of the RGD motif for binding.

In vitro there is a competition between CagL and classical extracellular matrix proteins like, e.g. fibronectin (Figs. 2, 4) in binding to integrins. Both fibronectin and CagL possess exposed RGD motifs that compete for integrin binding (Tegtmeyer et al. 2010). Integrin $\alpha_V\beta_3$ expressing WM-115 cells that were pre-incubated with either CagL or fibronectin display significantly reduced binding to immobilized fibronectin or CagL (Fig. 4). For the assay $CagL^{WT}$ was immobilized and WM-115 cells pre-incubated with varying concentrations of fibronectin were dispensed to the immobilized $CagL^{WT}$. Likewise, WM-115 cells were pre-incubated with different $CagL^{WT}$ concentrations before adding to immobilized fibronectin. Figure 4 displays reduced binding of WM-115 cells to immobilized fibronectin upon pre-incubation with $CagL^{WT}$ to about 90% at a concentration of 3.2 nM. This inhibition of cell adhesion was observed in a concentration-dependent manner. Vice versa, attachment of WM-115 cells pre-incubated with fibronectin to immobilized $CagL^{WT}$ was also inhibited.

The *spatial screening* concept that comprises the synthesis of a library of stereoisomeric cyclopeptides is a well-established approach for the development of new biologically active peptides. Cyclization leads to restriction of the peptide conformation. This concept is applied in search for an unknown bioactive conformation of a recognition sequence present in a ligand. The approach makes use of an array of synthetic cyclopeptides, where cyclization combined with incorporation of a secondary structure-inducing element results in the well-defined spatial presentation of the recognition sequence (Haubner et al. 1997; Xiong et al. 2002). The recognition epitope RGD has been combined with a secondary structure-inducing element, as for example a D-amino acid or a β-amino acid (Haubner et al. 1997; Schumann et al 2000; Urman et al. 2007; Royo Gracia et al. 2009). Several cyclic RGD peptides do not only display high affinity towards integrins, but also considerable selectivity between different integrin heterodimers. Hence, they are suited as tools for characterizing integrin–ligand interactions (Haubner et al. 1997; Weide et al. 2007; Royo Gracia et al. 2009). The cyclic pentapeptide c-(-Arg-Gly-Asp-D-Phe-Val-) is an example of an

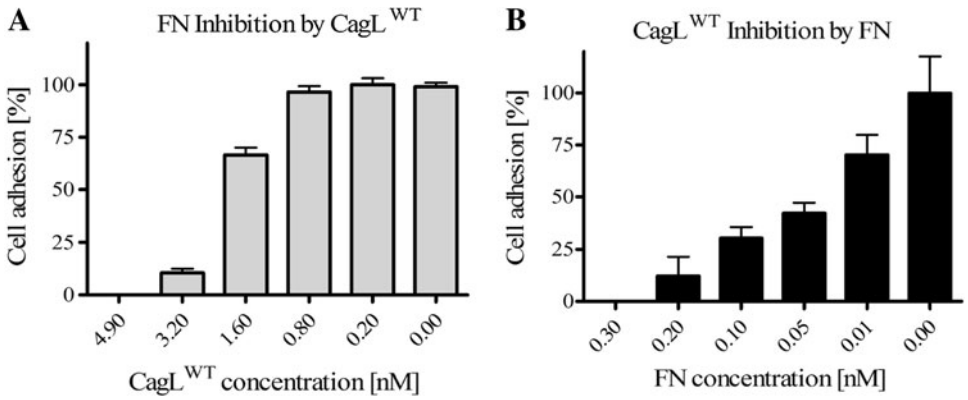

Fig. 4 Pre-incubation of WM-115 cells with either $CagL^{WT}$ (**a**) or fibronectin (FN) (**b**) inhibits binding to immobilized fibronectin (*left*) or immobilized $CagL^{WT}$ (*right*)

Table 7 Influence of peptides **1**–**7** on adhesion of WM-115 cells to $CagL^{WT}$, $CagL^{RAD}$, and $CagL^{RGA}$

Peptide		CagL	IC_{50} (95% CI) (μM)	R^2
1	c-(-Arg-Gly-Asp-D-Phe-Val-)	WT	0.32 (0.17–0.63)	0.90
		RAD	0.03 (0.01–46.4)	0.78
		RGA	0.43 (0.23–0.80)	0.90
2	c-(-Arg-Gly-Asp-D-Leu-Ala-)	WT	2.31 (1.40–3.82)	0.89
		RAD	1.63 (1.00–2.63)	0.93
		RGA	0.91 (0.58–1.43)	0.94
3	c-(-Arg-Gly-Asp-Leu-D-Ala-)	WT	0.81 (0.42–1.55)	0.87
		RAD	0.52 (0.24–1.12)	0.92
		RGA	0.96 (0.57–1.63)	0.92
4	c-(-Arg-Gly-Asp-D-Leu-Ala-Leu-)	WT	59.5 (30.2–117.5)	0.86
		RAD	23.0 (11.5–45.7)	0.88
		RGA	28.0 (14.1–55.6)	0.87
5	c-(-Arg-Gly-Asp-Leu-D-Ala-Leu-)	WT	22.8 (13.4–38.9)	0.90
		RAD	27.2 (16.8–43.9)	0.91
		RGA	15.6 (9.4–25.8)	0.93
6	c-(-Arg-Gly-Asp-Leu-Ala-D-Leu-)	WT	120 (73.3–195)	0.92
		RAD	57.1 (30.7–106)	0.90
		RGA	41.6 (23.3–74.3)	0.90
7	c-(-Arg-Ala-Asp-D-Leu-Ala-)	WT	388 (166–905)	0.72
		RAD	87.9 (58.1–133)	0.79
		RGA	242 (125–469)	0.73

integrin ligand that was developed by Kessler et al. in a *spatial screening* approach as a very active and selective ligand of integrin $\alpha_V\beta_3$ (Dechantsreiter et al. 1999; Lohof et al. 2000).

The target RGD sequence has been proposed to be found in an exposed loop of CagL, similar to the RGD motif of native integrin ligands like, e.g. fibronectin and vitronectin. Such exposed loops may be mimicked by small cyclic peptides. There is ample knowledge on the design principles of cyclic peptides in the *spatial screening* approach to provide selective high-affinity ligands for integrins like, e.g. $\alpha_{IIb}\beta_3$, $\alpha_V\beta_3$, and $\alpha_V\beta_5$. We chose synthetic cyclic RGD penta- and hexapeptides (Table 7) as tools for our investigations. Taking into account the selectivity of such peptides in binding to different integrins, this approach is suited for the characterization of the CagL–integrin interaction. The known cyclopeptide ligand c-(-Arg-Gly-Asp-D-Phe-Val-) **1** (Aumailley et al. 1991; Müller et al. 1994; Haubner et al. 1997) for integrin $\alpha_V\beta_3$ was included for comparison. Peptides **2**–**6** are derived from the CagL epitope -Ala-Leu-Arg-Gly-Asp-Leu-Ala- (Fig. 1) and additionally contain a D-amino acid. D-Amino acids are known to stabilize turn structures in cyclic peptides and preferably occupy the $i + 1$ position of a βII'-turn. Peptide **7** with the c-(-Arg-Ala-Asp-D-Leu-Ala-) sequence served as an RAD control peptide.

The linear precursors of the peptides were obtained by microwave-assisted solid-phase peptide synthesis on 2-chlorotrityl resin according to the Fmoc/tBu protection scheme. The linear peptides were cleaved from the resin and cyclized in solution under pseudo-high-dilution conditions using a dual syringe pump to avoid dimerization (Malešević et al. 2004). After deprotection of the permanent protecting groups the peptides were purified by RP-HPLC and characterized using MALDI-ToF MS. For structure–activity relationship studies the peptide conformations were determined with NMR and molecular dynamics (MD) calculations.

A cell adhesion assay was employed to investigate the influence of the peptides on binding of WM-115 cells to immobilized CagL and to quantify the inhibitory potencies of the different synthetic peptides (Fig. S2, Fig. 4). In order to elucidate the role and the structural requirements of the RGD motif for binding of CagL to integrins, the CagL mutants $CagL^{RAD}$ and $CagL^{RGA}$ were additionally employed.

In detail cyclic peptides **2**–**6** derived from CagL modulated adhesion of WM-115 cells to CagL with IC_{50} values in the nano- to micromolar range (Table 7). As expected, peptide **1**, a well-known high-affinity ligand for integrin $\alpha_V\beta_3$ inhibited the WM-115 cell adhesion to CagL with an IC_{50} value of 0.3 μM. IC_{50} values in the same range were obtained with **1** and the mutant $CagL^{RGA}$. The IC_{50} value for cell adhesion to $CagL^{RAD}$ is significantly lower (0.03 μM), emphasizing the importance of the glycine residue for CagL–integrin interactions. The CagL-derived cyclic pentapeptide **2** displayed a slightly higher IC_{50} value (2.3 μM) for adhesion to $CagL^{WT}$ and similar values for the mutants. The same is true for the CagL-derived cyclic pentapeptide **3** with IC_{50} values of 0.8 μM ($CagL^{WT}$), 0.5 μM ($CagL^{RAD}$), and 1.0 μM ($CagL^{RGA}$). In comparison with the cyclic pentapeptides, all three cyclic hexapeptides **4**–**6** displayed distinctly reduced effects on adhesion of WM-115 cells to CagL. The lower affinities of **4**–**6** (Table 7) are in accordance with previous results on cyclic RGD peptides, where higher affinity to integrin $\alpha_V\beta_3$ was observed for cyclic pentapeptides like **1** because of conformational reasons (Haubner et al. 1997; Gottschalk and Kessler 2002; Royo Gracia et al. 2009). Previous *spatial screening* studies have shown that integrin $\alpha_V\beta_3$ preferentially binds peptides like **1** that present a bent RGD sequence, e.g. a γ-turn around Gly (Haubner et al. 1997; Gottschalk and Kessler 2002). The cell adhesion assays with mutants $CagL^{RAD}$ and $CagL^{RGA}$ revealed similar or slightly improved influence of the cyclopeptides on cell adhesion (Table 7). This corroborates the hypothesis that CagL–$\alpha_V\beta_3$ interaction partly relies on RGD recognition like previously communicated for $\alpha_5\beta_1$ (Kwok et al. 2007), but additionally involves

Table 8 Number of clusters and their population during unrestrained MD calculations

Peptide		Number of clusters (population)
2	c-(-Arg-Gly-Asp-D-Leu-Ala-)	2 (80%, 16%)
3	c-(-Arg-Gly-Asp-Leu-D-Ala-)	2 (85%, 8%)
4	c-(-Arg-Gly-Asp-D-Leu-Ala-Leu-)	3 (41%, 13%, 8%)
5	c-(-Arg-Gly-Asp-Leu-D-Ala-Leu-)	1 (84%)
6	c-(-Arg-Gly-Asp-Leu-Ala-D-Leu-)	3 (41%, 16%, 14%)
7	c-(-Arg-Ala-Asp-D-Leu-Ala-)	2 (84%, 86%)

Only clusters containing equal or more than 8% of the trajectory were considered

an additional epitope within CagL that remains to be identified.

Structure proposals

Conformational analysis of the cyclic peptides by NMR spectroscopy relied on distance information obtained from NOE or ROE experiments, which were subsequently used in molecular dynamics calculations (MD). The analysis was performed according to the workflow given in the Supplementary Material, Figure S1.

The structures of the trajectories during the MD calculations were clustered according to the backbone torsion angles (Guthöhrlein et al. 2007). The numbers of clusters of the unrestrained MD calculations are listed in Table 8. The overlays of the resulting structures are displayed in Fig. 5. For the structure proposal only unrestrained MD clusters with a minimum population of 8% were considered. One cluster was found for peptide **5**, while the structures of cyclic peptides **2**, **3**, **4**, and **7** gave two or three clusters differing by single peptide bond reorientations only, mainly in the vicinity of the flexible glycine residue. For peptide **6** one of the clusters differs considerably from the other two. However, this conformation is not supported by either the temperature gradients $\Delta\delta/\Delta T$ of the NH proton chemical shifts or the coupling constants. As expected, the D-amino acids are found in the $i + 1$ position of βII'-turns except for peptide **3**. However, in this peptide a Gly residue resides there (see below).

The torsion angles of the peptides (Table 9) determine their secondary structure elements discussed below, which

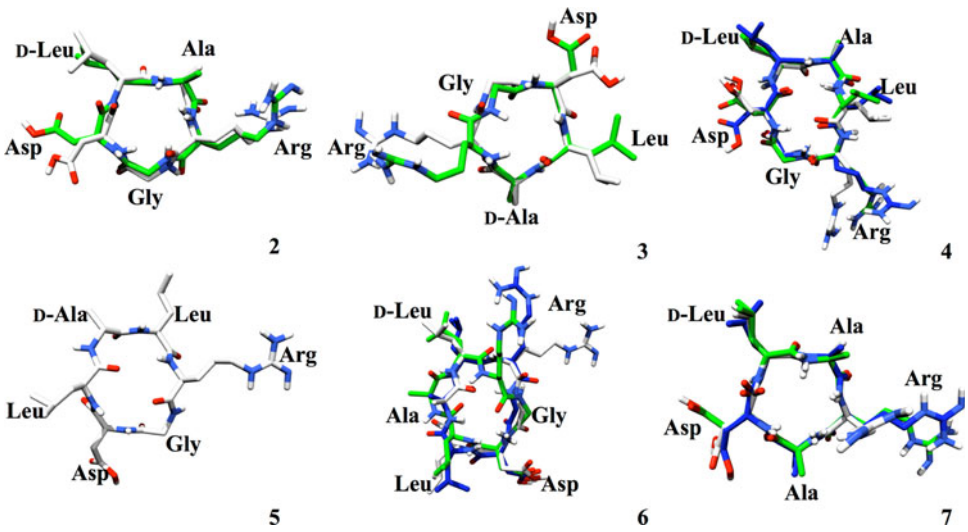

Fig. 5 Clusters obtained for peptides **2–7** after unrestrained MD calculations

Table 9 Torsion angles observed in the central structures of the first clusters of peptides **2–7** after unrestrained MD calculations

Amino acid	Peptide **2**		Peptide **3**		Peptide **4**		Peptide **5**		Peptide **6**		Peptide **7**	
	φ	ψ	φ	ψ	φ	ψ	φ	ψ	φ	ψ	φ	ψ
Arg	−119	103	−109	99	−51	−116	101	116	−107	119	−111	−62
Gly/Ala	90	−76	115	−87	123	177	−107	−67	80	−104	−104	−50
Asp	−130	105	−98	−57	−131	−118	−48	133	−116	−39	−127	109
Leu	118	−98	−128	101	68	−119	−22	−109	−105	134	111	−85
Ala	−104	−51	100	−88	−98	−129	129	−29	75	−124	−86	−52
Leu					−102	76	−115	152	−105	−33		

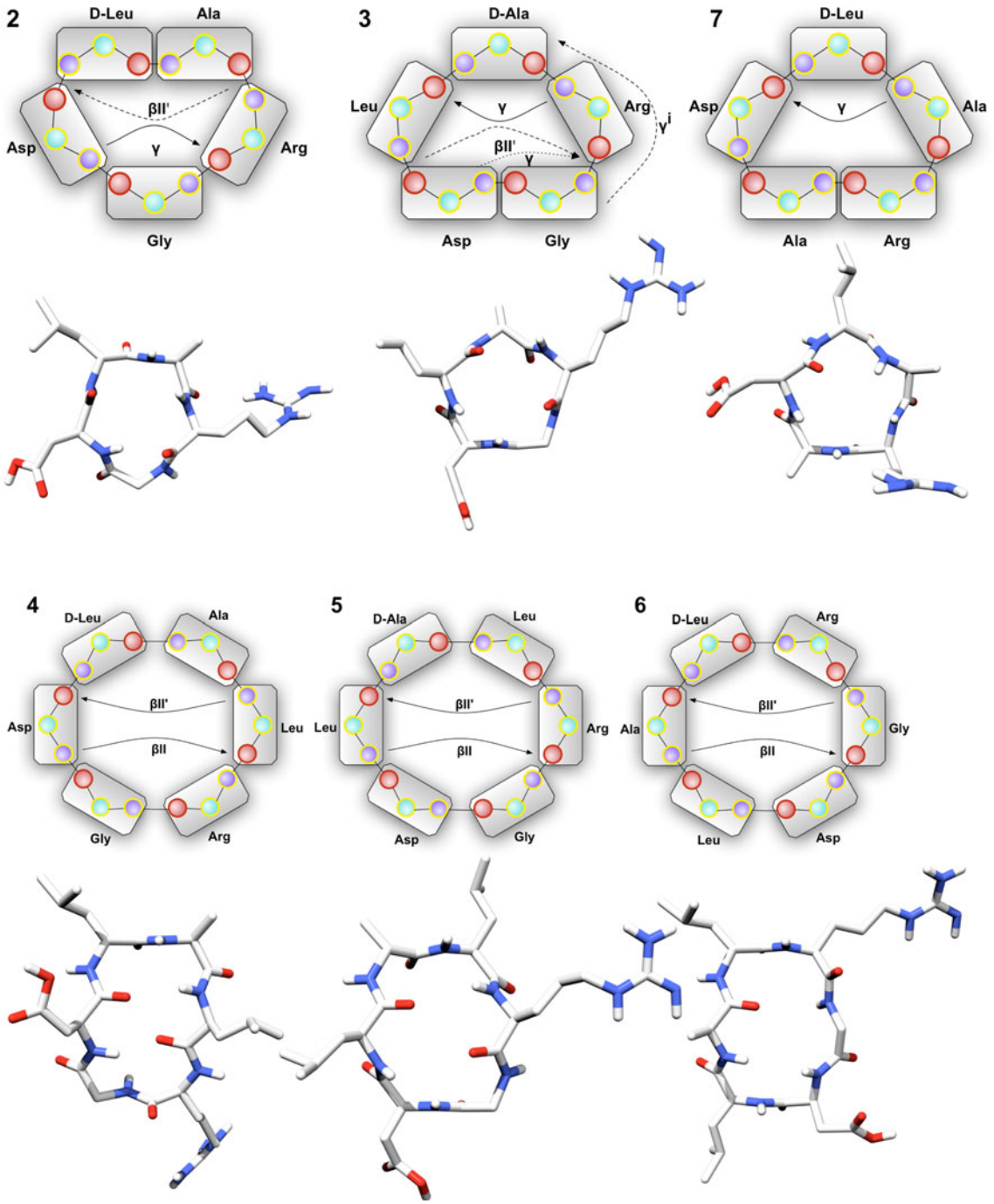

Fig. 6 Structures of cyclic peptides **2–7** in DMSO: unrestrained MD main cluster and schematic representation of the structures of peptides **2–7**, respectively

are additionally supported by a good agreement of hydrogen bonds observed during the MD trajectories with the temperature gradients $\Delta\delta/\Delta T$ of the corresponding amide proton chemical shifts. In addition, the coupling constants as determined from 1D ^{1}H NMR spectra are compared with the coupling constants calculated from the torsion angles observed in the structure proposal (Supplementary Material Tables S8–S12).

According to the conformational analysis performed by NMR/MD calculations in DMSO, **2** clearly reproduces the expected structural features of peptide **1** such as a βII'-turn with D-Leu in $i + 1$ position and a γ-turn around Gly

(Fig. 6). Peptide **3** appears to be more flexible than **1** and **2**. The D-amino acid D-Ala is not found in $i + 1$ position of a βII'-turn, but in the central position of a γ-turn. A βII'-turn with Gly in $i + 1$ position is nested with a γ-turn around Gly. This results in a kinked RGD sequence and provides a similar 3D-presentation of the RGD sequence like in **2**, especially with respect to orientation of the Arg $C^{\alpha} \rightarrow C^{\beta}$ and Asp $C^{\alpha} \rightarrow C^{\beta}$ vectors, which explains the comparable affinity of **2** and **3** (Table 7).

The orientation of the Arg $C^{\alpha} \rightarrow C^{\beta}$ and Asp $C^{\alpha} \rightarrow C^{\beta}$ vectors also correlates partially with the distances between C^{α} of Arg and Asp as well as C^{β} of Arg and Asp, respectively (Müller et al. 1994). Interestingly for **2** and **3**, the distance Arg $C^{\alpha} \rightarrow$ Asp C^{α} varies in the range 500–700 pm during the trajectory. The distance Arg $C^{\beta} \rightarrow$ Asp C^{β} is also similar in peptides **2** and **3**, varying between 700 and 900 pm during the trajectory with an average value of 800 and 850 pm, respectively. Both distances are only slightly longer than those observed for the known integrin ligand **1** (Arg $C^{\alpha} \rightarrow$ Asp C^{α}: 550 pm; Arg $C^{\beta} \rightarrow$ Asp C^{β}: 670 pm) (Müller et al. 1994). According to NMR/MD studies and X-ray analysis, the structures of Cilengitide™, the *N*-methyl valine analog of **1**, either unbound or in complex with integrin $\alpha_V\beta_3$ are also similar (Xiong et al. 2002; Gottschalk and Kessler 2002). In this highly active peptide, the distance Arg $C^{\beta} \rightarrow$ Asp C^{β} is very similar to the distance observed in peptides **2** and **3**, ranging from 800 to 850 pm (Dechantsreiter et al. 1999). Thus, the affinity of peptides **2** and **3** to integrin $\alpha_V\beta_3$ agrees well with the known structure–activity relationship (Müller et al. 1994).

Peptide **7** has only one secondary structural element, a γ-turn around D-Leu, like that seen in peptide **3** around the D-amino acid Ala. Though peptide **7** is about 500–1,000 fold less active than peptides **1**–**3**, the distances between C^{α} of Arg and Asp and C^{β} of Arg and Asp (Arg $C^{\alpha} \rightarrow$ Asp C^{α}: 500–680 pm; Arg $C^{\beta} \rightarrow$ Asp C^{β}: 650–900 pm) are comparable. The missing structural features may be one reason for the loss of activity, but most probably the additional methyl group is unfavorable for tight receptor binding. Presumably, receptor residues sterically hinder binding and need the glycine residue in the RGD recognition sequence (Müller et al. 1994).

The structural analysis of the CagL hexapeptides in DMSO yielded structure proposals which correspond well to the expected preference of D-amino acids for the $i + 1$ position of a βII'-turn (Fig. 6). In peptides **4** and **5** Gly occupies the $i + 1$ or the $i + 2$ position of a βII-turn, respectively, resulting in somewhat kinked RGD motifs. An elongated RGD sequence is observed for peptide **6**, Arg is found in $i + 2$ position of a βII'-turn and Asp in $i + 1$ position. The RGD motif has an unfavorable structure for integrin binding and this explains the reduced affinity of **6** in comparison with **4** and **5**. Moreover, this explains the higher micromolar IC_{50} values of cyclohexapeptides, whereas the cyclopentapeptides are more active. This underscores the importance of the three-dimensional structure of the RGD pharmacophore.

Conclusions

We had previously shown that the *H. pylori* protein CagL is able to bind to integrin $\alpha_5\beta_1$. The cell adhesion assays with different murine monoclonal antibodies show that recombinant CagL also binds to $\alpha_V\beta_3$, and to some extent to $\alpha_V\beta_5$. These interactions can be inhibited with RGD peptides derived from CagL that have been designed as ligands with a specific conformational match for integrin $\alpha_V\beta_3$. Structure–activity relationship studies demonstrate the distinct influence of the peptide conformation on their ability to interfere with this interaction, proposing similar structural requirements for the binding site of CagL as previously suggested for binding of other ligands to integrin $\alpha_V\beta_3$ (Müller et al. 1994). The affinity of the peptides toward integrin $\alpha_V\beta_3$ and, consequently, the inhibitory effect on the CagL–$\alpha_V\beta_3$ interaction mainly depends on secondary structure elements, where a kinked Arg-Gly-Asp recognition motif is favored. The kinked RGD motif can be found in cyclopentapeptides with a D-Xaa[4] amino acid in $i + 1$ position of a βII'-turn and a γ-turn around the Arg-Gly-Asp recognition sequence. These structural elements are found in peptide **2** like in the prototype peptide **1**. In peptide **3** the D-Ala forms a γ-turn in $i + 2$ position and induces a βII'-turn around Gly-Asp nested with a γ-turn that leads to a kinked Arg-Gly-Asp motif as well. The cyclic hexapeptides have a more stretched Arg-Gly-Asp motif and are more flexible. This prevents tight binding and results in considerably higher IC_{50} values. The inhibition of the CagL–integrin interaction by RGD peptides strongly suggests the importance of the Arg-Gly-Asp recognition sequence for CagL binding. In addition, the data obtained for the $CagL^{RAD}$ and $CagL^{RGA}$ mutants lead to the conclusion that presumably an additional CagL epitope is involved in binding to integrins $\alpha_V\beta_3$ and $\alpha_5\beta_1$.

Acknowledgments The authors thank Carmela Michalek and Marco Wißbrock for skillful technical assistance. Financial support came from the NRW Graduate School in Bioinformatics and Genome Research, Bielefeld University (PhD Fellowship to K.G.), the EU (Marie Curie Fellowship to S.R.G.), and Deutsche Forschungsgemeinschaft, which is gratefully acknowledged.

Conflict of interest The authors declare that they have no conflict of interest.

References

Amieva MR, El-Omar EM (2008) Host-bacterial interactions in *Helicobacter pylori* infection. Gastroenterol 134:306–320

Asahi M, Azuma T, Ito S, Ito Y, Suto H, Nagai Y, Tsubokawa M, Tohyama Y, Maeda S, Omata M, Suzuki T, Sasakawa CJ (2000) *Helicobacter pylori* CagA protein can be tyrosine phosphorylated in gastric epithelial cells. Exp Med 191:593–602

Aumailley M, Gurrath M, Müller G, Calvete J, Timpl R, Kessler H (1991) Arg-Gly-Asp constrained with cyclic pentapeptides. FEBS Lett 291:50–54

Backert S, Meyer TF (2006) Type IV secretion systems and their effectors in bacterial pathogenesis. Curr Opin Microbiol 9:207–212

Backert S, Selbach M (2008) Role of type IV secretion in *Helicobacter pylori* pathogenesis. Cell Microbiol 10:1573–1581

Backert S, Ziska E, Brinkmann V, Zimny-Arndt U, Faucinnier A, Jungblut PR, Neumann M, Meyer TF (2000) Translocation of the *Helicobacter pylori* CagA protein in gastric epithelial cells by a type IV secretion apparatus. Cell Microbiol 2:155–164

Backert S, Fronzes R, Waksman G (2008) VirB2 and VirB5 proteins: specialized adhesins in bacterial type-IV secretion systems? Trends Microbiol 16:409–413

Bax A, Davis DG (1985a) Practical aspects of two-dimensional transverse NOE spectroscopy. J Magn Reson 63:207–213

Bax A, Davis DG (1985b) MLEV-17-based two-dimensional homonuclear magnetization transfer spectroscopy. J Magn Reson 65:355–360

Bax A, Summers MFJ (1986) ^{1}H and ^{13}C assignments from sensitivity-enhanced detection of heteronuclear multiple-bond connectivity by 2D multiple quantum NMR. J Am Chem Soc 108:2093–2094

Bourzac KM, Guillemin K (2005) *Helicobacter pylori*–host cell interactions mediated by type IV secretion. Cell Microbiol 7:911–919

Cascales E, Christie PJ (2003) The versatile bacterial type IV secretion systems. Nat Rev Microbiol 1:137–149

Charo IF, Nannizzi L, Smith JW, Cheresh DA (1990) The vitronectin receptor $\alpha_V\beta_3$ binds fibronectin and acts in concert with $\alpha_5\beta_1$ in promoting cellular attachment and spreading on fibronectin. J Cell Biol 111:2795–2800

Dechantsreiter MA, Planker E, Mathä B, Lohof E, Hölzemann G, Jonczyk A, Goodman SL, Kessler H (1999) N-methylated cyclic RGD peptides as highly active and selective $\alpha_V\beta_3$ integrin antagonists. J Med Chem 42:3033–3040

Eble JA, Kühn K (eds) (1997) Integrin-ligand interaction. Springer, Heidelberg

Geerke DP, Oostenbrink C, van der Vegt NFA, van Gunsteren WF (2004) An effective force field for molecular dynamics simulations of dimethyl sulfoxide and dimethyl sulfoxide-water mixtures. J Phys Chem B 108:1436–1445

Goddard TD, Kneller DG, Sparky 3, University of California, San Francisco

Gottschalk K-E, Kessler H (2002) The structures of integrins and integrin-ligand complexes: implications for drug design and signal transduction. Angew Chem Int Ed 41:3767–3774

Guthöhrlein EW, Malešević M, Majer Z, Sewald N (2007) Secondary structure inducing potential of ß-amino acids: torsion angle clustering facilitates comparison and analysis of the conformation during MD trajectories. Biopolymers 88:829–839

Haubner R, Finsinger D, Kessler H (1997) Stereoisomeric peptide libraries and peptidomimetics for designing selective inhibitors of the $\alpha_V\beta_3$ integrin for a new cancer therapy. Angew Chem Int Ed 36:1374–1389

Hoffmann C, Ohlsen K, Hauck CR (2011) Integrin-mediated uptake of fibronectin-binding bacteria. Eur J Cell Biol. doi: 10.1016/j.ejcb.2011.03.001

Isberg RR, Barnes PJ (2001) Subversion of integrins by enteropathogenic *Yersinia*. Cell Sci 114:21–28

Isberg RR, Leong JM (1990) Multiple β_1 chain integrins are receptors for invasin, a protein that promotes bacterial penetration into mammalian cells. Cell 60:861–871

Isberg RR, Tran Van Nhieu G (1994) Binding and internalization of microorganisms by integrin receptors. Trends Microbiol 2:10–14

Jackson T, Sheppard D, Denyer M, Blakemore W, King AMQ (2000) The epithelial integrin $\alpha_V\beta_6$ is a receptor for foot-and-mouth disease virus. J Virol 74:4949–4956

Jackson T, Mould AP, Sheppard D, King AMQ (2002) Integrin $\alpha_V\beta_1$ is a receptor for foot-and-mouth disease virus. J Virol 76:935–941

Jiménez-Soto LF, Kuttner S, Sewald X, Ertl C, Weiss E, Kapp U, Rohde M, Pirch T, Jung K, Retta SF, Terradot L, Fischer W, Haas R (2009) *Helicobacter pylori* type IV secretion apparatus exploits β1 integrin in a novel RGD-independent manner. PLoS Pathog 5(12):e1000684

Kay LE, Keifer P, Saarinen T (1992) Pure absorption gradient enhanced heteronuclear single quantum correlation spectroscopy with improved sensitivity. J Am Chem Soc 114:10663–10665

Kwok T, Backert S, Schwarz H, Berger J, Meyer TF (2002) Specific Entry of *Helicobacter pylori* into cultured gastric epithelial cells via a zipper-like mechanism. Infect Immun 70:2108–2120

Kwok T, Zabler D, Urman S, Rohde M, Hartig R, Wessler S, Misselwitz R, Berger J, Sewald N, König W, Backert S (2007) Helicobacter exploits integrin for type IV secretion and kinase activation. Nature 449:862–866

Lohof E, Planker E, Mang C, Burkhart F, Dechantsreiter MA, Haubner R, Wester H-J, Schwaiger M, Hölzemann G, Goodmann SL, Kessler H (2000) Carbohydrate derivatives for use in drug design:cyclic α_V-selective RGD peptides. Angew Chem Int Ed 39:2761–2764

Macura S, Huang Y, Suter D, Ernst RR (1981) Two-dimensional chemical exchange and cross-relaxation spectroscopy of coupled nuclear spins. J Magn Reson 43:259–281

Malešević M, Strijowski U, Bächle D, Sewald N (2004) An improved method for the solution cyclization of peptides under pseudo-high dilution conditions. J Biotechnol 112:73–77

Markley JL, Bax A, Arata Y, Hilbers CW, Kaptein R, Sykes BD, Wright PE, Wüthrich K (1998) Recommendations for the presentation of NMR structures of proteins and nucleic acids. J Biomol NMR 12:1–23

Mas-Moruno C, Rechenmacher F, Kessler H (2010) Cilengitide:the first anti-angiogenic small molecule drug candidate design, synthesis and clinical evaluation. Anti Canc Agents Med Chem 10:753–768

Meyer A, Auernheimer J, Modlinger A, Kessler H (2006) Targeting RGD recognizing integrins: drug development, biomaterial research, tumor imaging and targeting. Curr Pharm Des 12:2723–2747

Müller G, Gurrath M, Kessler H (1994) Pharmacophore refinement of gpIIb/IIIa antagonists based on comparative studies of antiadhesive cyclic and acyclic RGD peptides. J Comp Aided Mol Des 8:709–730

Pierschbacher MD, Hayman EG, Ruoslahti E (1981) Location of the cell-attachment site in fibronectin with monoclonal antibodies and proteolytic fragments of the molecule. Cell 26:259–267

Rance M, Sørensen OW, Bodenhausen G, Wagner G, Ernst RR, Wüthrich K (1983) Improved spectral resolution in cosy ^{1}H NMR spectra of proteins via double quantum filtering. Biochem Biophys Res Commun 117:479–485

Rieder G, Fischer W, Haas R (2005) Interaction of *Helicobacter pylori* with host cells: function of secreted and translocated molecules. Curr Opin Microbiol 8:67–73

Royo Gracia S, Gaus K, Sewald N (2009) Synthesis of chemically modified bioactive peptides: recent advances, challenges and developments for medicinal chemistry. Future Med Chem 1:1289–1310

Ruoslahti E (1996) RGD and other recognition sequences for integrins. Annu Rev Cell Dev Biol 12:697–715

Ruoslahti E, Pierschbacher MD (1987) New perspectives in cell adhesion: RGD and integrins. Science 238:491–497

Schuler LD, Daura X, van Gunsteren WF (2001) An improved GROMOS 96 force field for aliphatic hydrocarbons in the condensed phase. J Comput Chem 22:1205–1218

Schumann F, Müller A, Koksch M, Müller G, Sewald N (2000) Are β-amino acids γ-turn mimetics?—exploring a new design principle for bioactive cyclopeptides. J Am Chem Soc 122:12009–12010

Schwieters CD, Kuszewski JJ, Tjandra N, Clore GM (2003) The Xplor-NIH NMR molecular structure determination package. J Magn Res 160:65–73

Serini G, Valdembri D, Bussolino F (2006) Integrins and angiogenesis: a sticky business. Exp Cell Res 312:651–658

Shaka A, Lee CJ, Davis DG (1988) Iterative schemes for bilinear operators; application to spin decoupling. J Magn Reson 77:274–293

Sheppard D (2003) Functions of pulmonary epithelial integrins: from development to disease. Physiol Rev 83:673–686

Stewart PL, Nemerow GR (2007) Cell integrins: commonly used receptors for diverse viral pathogens. Trends Microbiol 15:500–507

Tegtmeyer N, Hartig R, Delahay RM, Rohde M, Brandt S, Conradi J, Takahashi S, Smolka AJ, Sewald N, Backert S (2010) A small fibronectin-mimicking protein from bacteria induces cell spreading and focal adhesion formation. J Biol Chem 285:23515–23526

Urman S, Gaus K, Yang Y, Strijowski U, De Pol S, Reiser O, Sewald N (2007) β-ACC containing RGD peptides efficiently inhibit tumor cell adhesion. Angew Chem Int Ed 46:3976–3978

Weide T, Modlinger A, Kessler H (2007) Spatial screening for the identification of the bioactive conformation of integrin ligands. Top Curr Chem 272:1–50

Wickham TJ, Filardo EJ, Cheresh DA, Nemerow GR (1994) Integrin $\alpha_V\beta_5$ selectively promotes adenovirus mediated cell membrane permeabilization. J Cell Biol 127:257–264

Xiong J-P, Stehle T, Zhang R, Joachimiak A, Frech M, Goodman SL, Arnaout MA (2002) Crystal structure of the extracellular segment of integrin alpha V beta3 in complex with an Arg-Gly-Asp ligand. Science 296:151–155